Surface fluctuations at the liquid-liquid interface

Janamejaya Chowdhary* and Branka M. Ladanyi†
Department of Chemistry, Colorado State University, Fort Collins, Colorado 80523, USA
(Received 20 November 2007; published 24 March 2008)

Within the capillary-wave model (CWM), the liquid-vapor interface is a hypothetical two-dimensional surface whose deviations from planarity are represented as long wavelength capillary waves. We modify the CWM for liquid-liquid interfaces and treat them as two harmonically interacting surfaces (model 1). Corrections to the model are proposed to prevent the usual divergence of the capillary-wave broadening in the thermodynamic limit by introducing a surface-bulk coupling (model 2) and to incorporate the curvature of the two surfaces (model 3). Expressions for the capillary-wave contribution to the surface tension of the interface are obtained. Molecular dynamics simulations are performed for two series of water-hydrocarbon interfacial systems (a) *n*-pentane, 2-methyl pentane, and 2,2,4-trimethyl pentane (constant chain length) and (b) *n*-octane, 2-methyl heptane, and 2,2,4-trimethyl pentane (constant molecular mass). A simple procedure to identify the molecular sites at the surface is utilized for a molecular representation of the surface. The distribution of these surface sites as well as the wave-vector dependence of surface fluctuations are analyzed in order to extract the parameters required for model 2. A small length scale is identified above which surface fluctuations correspond to capillary-wave fluctuations thereby connecting the molecular and mesoscopic scales. This approach is applied to all interfacial systems studied here and predictions based on the parameters found to be in good agreement with independent simulation results for surface tension and interfacial widths. Hydrocarbon branching has a small effect on model parameters.

DOI: 10.1103/PhysRevE.77.031609 PACS number(s): 68.05.−n

I. INTRODUCTION

Interfaces are common in nature as well as important in numerous industrially significant processes. An understanding of their properties [1] is therefore particularly useful. The breakdown of translational symmetry at the interface leads to long-wavelength thermally activated capillary waves (CW) that account for fluctuations of the surface. Buff *et al.* [2] incorporated these surface modes into their capillary-wave model (CWM) for liquid-vapor interfaces. A key prediction of the CWM is the divergence of the width of this surface due to CW in the thermodynamics limit. Furthermore, inclusion of an external field, e.g., gravity, leads to a width that diverges in the limit of vanishing field strength. These predictions could be unphysical and the CWM is a matter of some controversy [3,4].

In the context of liquid-liquid interfaces, direct transferability and application without modification of ideas from liquid-vapor systems is typically assumed [5]. While this seems at first to be a reasonable assumption (and indeed the resulting predictions are apparently consistent with simulation studies, e.g., Ref. [6]), it has its shortcomings. The location of a liquid-vapor interface is typically represented by the position of the Gibbs surface obtained from the one-dimensional density profile [7]. For the liquid-liquid interface, a Gibbs surface can be identified for each liquid forming the interface. The positions of the two Gibbs surfaces so obtained do not necessarily coincide for most liquid-liquid interfaces and this manifests itself as a depletion zone at the interface in the total density profile (defined as the sum of the density profiles for the two liquid components forming the interface), e.g., in water-hydrocarbon interfaces [8,9], unlike the liquid-vapor interface where this depletion zone is absent. Clearly, selecting a single Gibbs surface for the liquid-liquid interface is ambiguous and a better representation of the interface includes two interacting surfaces, one for each component of the liquid-liquid interface. One objective of this paper is therefore to formulate new model phenomenological Hamiltonians that can account for fluctuations of the two surfaces forming the liquid-liquid interface.

With these Hamiltonians available, analytic expressions for average surface characteristics such as width, distribution of surface positions, and wave-vector dependence of fluctuations can be derived. Computer simulations provide a direct means of studying liquid-liquid interfaces and allow for a numerical identification of molecular sites representative of the surface at the interface. While a surface can be identified by partitioning the interface into grids and identifying the local Gibbs surface based on the density profile for each grid, there is no one to one correspondence with the physical atoms or molecules at the surface. Furthermore, it has been shown that the local Gibbs surface leads to fluctuations dominated by bulk fluctuations at small length scales [10,11]. In view of these observations, we abandon the representation of the surface of each liquid by the local Gibbs surface. Instead, we note that the set of discrete molecular sites at the surface of each liquid is another physical realization of the surface and capillary-wave fluctuations are now associated with changes in configuration of molecules at both surfaces. In our study of the intrinsic structure of water-hydrocarbon interfaces [12] we had presented a procedure for identification of the surface sites. An analysis of these surface sites and the CW fluctuations inherent in them will be interpreted in terms of the models presented here.

*janamej@lamar.colostate.edu
†Branka.Ladanyi@colostate.edu

Since the CWM is mesoscopic in nature and applicable to a coarse grained interface, it is important to connect the molecular and mesoscopic pictures by identifying the smallest length scale (L_m) above which this model can be applied. There is neither a formal prescription for determining the magnitude of L_m nor a consensus on the choice or its magnitude in the literature. A physical interpretation of L_m would make most sense if it were related to some characteristic length scale associated with the molecules or the bulk liquid structure. Some of the commonly used definitions of L_m are correlation length [7] (n-nonane/water $\simeq$6 Å [13], isooctane/water $\simeq$6.5 Å [14]), diameter of molecule for the smaller (n-octane/water $\simeq$3 Å [15]) or larger (n-hexane/water $\sim$4 Å [8]) of the two molecules forming the interface, and the average separation between the molecules (CCl_4/water $\simeq$4.3 Å [6]). In view of this uncertainty in estimating L_m, another objective of this paper is to provide a numerical approach that can be applied to any interfacial system.

Previously, we have studied the effect of hydrocarbon branching on the intrinsic structure of water-hydrocarbon interfaces [12]. A secondary objective in this work is therefore to obtain model parameters from an analysis of the surface sites for different water-hydrocarbon interfaces. The variation of these parameters with hydrocarbon branching then sheds light on its effect on the interface.

This paper is organized as follows. In Sec. II we summarize the CWM and present extensions for the liquid-liquid interface, taking into account coupling between the two surfaces (model 1), the effect of surface-bulk interactions (model 2), and curvature corrections (model 3). As pointed out by Kayser [16], the capillary waves contribute to the value of the total surface tension of the system. The CW contribution to the surface tension as well as the total surface tension of the interface is also presented in this section. In Sec. III we present the summary of our simulation methodology and surface layer identification. Section IV contains the analysis of surface positions and a test of the predictions of model 2. Finally, the main results are summarized and their implications discussed in Sec. V.

II. THEORETICAL MODELS

A. Capillary-wave model

For density variation from the vapor to the liquid phase along the z direction, the CWM postulates an instantaneous nonplanar surface $z=\xi(\mathbf{r})$, where $\mathbf{r}=(x,y)$, arising due to capillary waves unfrozen on a reference planar surface. The Hamiltonian for the system, H_{CW}, can be written as the work done in changing the surface area from its reference to the instantaneous value [2]. Weeks and van Saarloos [17] have shown that the same CW Hamiltonian can be obtained via the density-functional theory and corresponds to the change in free energy due to surface fluctuations. In this sense, the CW Hamiltonian is a Landau-Ginzburg-type Hamiltonian.

For a reference square surface with edge L centered at $z=\langle\xi(\mathbf{r})\rangle=0$ and a constant wave-vector (q) independent surface tension, $\gamma(q)=\gamma(0)=\gamma_0$, one obtains

$$H_{CW}=\gamma_0\int \mathbf{dr}\{\sqrt{1+|\nabla\xi(\mathbf{r})|^2}-1\}, \tag{1}$$

where $\nabla=\hat{e}_x\frac{\partial}{\partial x}+\hat{e}_y\frac{\partial}{\partial y}$ and $\hat{e}_x$ is the unit vector along the x direction. Introducing the two-dimensional (2D) Fourier series representation of the instantaneous surface, $\xi(\mathbf{r})=\Sigma_{\mathbf{q}\neq\mathbf{0}}\hat{\xi}_{\mathbf{q}}\exp(i\mathbf{q}\cdot\mathbf{r})$, where $\mathbf{q}=\frac{2\pi}{L}(n_x\hat{e}_x+n_y\hat{e}_y)$ and $n_x,n_y=0,\pm1,\pm2,\ldots\pm\infty$, for small deviations from planarity, the Hamiltonian can be rewritten as

$$H_{CW}=\frac{1}{2}\gamma_0L^2\sum_{\mathbf{q}\neq\mathbf{0}}q^2|\hat{\xi}_{\mathbf{q}}|^2, \tag{2}$$

and using the equipartition theorem leads to

$$\langle|\hat{\xi}_{\mathbf{q}}|^2\rangle=(\beta L^2\gamma_0q^2)^{-1}, \tag{3}$$

where $\beta^{-1}=k_bT$ and k_b is the Boltzmann constant.

With the Hamiltonian available, analytic expressions for a number of interfacial properties can be obtained. An important feature of the interface is its roughness, which can be quantified by the width of the interface, σ^2_{CW}, defined as the variance of the capillary-wave contribution to the distribution of surface positions, and can be obtained from x-ray or neutron reflectivity experiments [18]. This can be expressed as the sum of mean squared amplitudes, for all allowed $\mathbf{q}$, and one obtains

$$\sigma^2_{CW}=\sum_{\mathbf{q}\neq0}\langle|\hat{\xi}_{\mathbf{q}}|^2\rangle=\frac{1}{2\pi\gamma_0\beta}\int_{q_{\min}}^{q_{\max}}dq\frac{1}{q}=\frac{1}{2\pi\gamma_0\beta}\ln\left(\frac{L}{L_m}\right). \tag{4}$$

The small wavelength limit is $q_{\min}=2\pi/L$, where L is the linear dimension of the system in the xy plane. Divergence of the integral over q is avoided by introducing a large wavelength cutoff $q_{\max}=2\pi/L_m$, where L_m corresponds to a small length scale above which the CWM applies. Due to the introduction of L_m, the CW Hamiltonian can be thought of as a coarse grained Hamiltonian where the contribution of surface fluctuations with wavelengths larger than $2\pi/L_m$ have been implicitly incorporated into the surface tension, which is referred to as the "bare" surface tension. This bare surface tension was shown [17] to be equivalent to the Triezenberg-Zwanzig expression for surface tension [19]. The surface tension γ_0, occurring in Eq. (4), should be interpreted as a bare surface tension and not as the macroscopic surface tension. The total surface tension of the interface can be expressed as the sum of the bare surface tension corresponding to surface fluctuations with a wavelength larger than $2\pi/L_m$ and a capillary-wave contribution due to fluctuations with wavelengths smaller than $2\pi/L_m$ as pointed out by Kayser [16].

In addition to the width of the interface, another quantity of particular relevance is the height-height correlation function $\langle\xi(\mathbf{0})\xi(\mathbf{r})\rangle$ for the interface. The contribution of interfacial height fluctuations to the differential cross section for x-ray diffraction in the distorted-wave Born approximation [18] is directly proportional to the Fourier transform of the height-height correlation function, which in general can be written as

$$\langle|\hat{\xi}_{\mathbf{q}}|^2\rangle = \frac{1}{\beta L^2}\frac{1}{H(q)}, \tag{5}$$

and a comparison with Eq. (3) gives $H(q)=\gamma_0 q^2$ for the CWM. Inclusion of curvature corrections to the Hamiltonian, as done by Helfrich [20], by incorporating the bending rigidity of the interface, κ, leads to the result $H(q)=\gamma(q)q^2$, where $\gamma(q)=\gamma_0+\kappa q^2$ is the wave-vector-dependent surface tension. A recent density-functional theory by Mecke *et al.* [21] predicts a $\gamma(q)$ that decreases from the macroscopic value γ_0 to a minimum followed by an increase of the form $\kappa_1 q^2$ for large q, where $\kappa_1>0$. Recent experimental measurements [22–24] and some computer simulations [10,11] of $\gamma(q)$ have been successfully interpreted in terms of the Mecke *et al.* theory [21] for a number of molecular and metallic liquid-vapor interfaces. On the other hand, other theoretical work [25] suggests that $\gamma(q)$ should have an inverse q^2 dependence and this appears to be the case in other simulation studies [25–28]. The discrepancy could be due to different definitions of the interface or due to negative bending rigidity in simulations [25].

B. Model 1: Coupled surfaces

Let $\xi_A(\mathbf{r})$ and $\xi_B(\mathbf{r})$ be the positions of the surface for liquids A and B that form the liquid-liquid interface and let them represent the lower and upper surfaces at the interface, respectively. We limit our attention to thermodynamic states at which the two liquids are not miscible and form a well defined interface. Let the bare surface tension values for the two surfaces be γ_{A0} and γ_{B0}. For an equilibrium system, $\gamma_{A0}\simeq\gamma_{B0}$. Upon unfreezing the CW's in the system, one would expect the CW broadened width of the two surfaces to be equal, i.e., $\sigma^2_{CW}(A)\simeq\sigma^2_{CW}(B)$. However, we will continue using distinct values for the surface tensions of the two surfaces until the final results are presented.

Just as for the CWM for liquid-vapor interfaces, we start by expressing the positions of the two surfaces as a 2D Fourier series

$$\xi_A(\mathbf{r}) = \xi_{A0} + \sum_{\mathbf{q}\neq\mathbf{0}} \hat{\xi}_{A,\mathbf{q}} \exp(i\mathbf{q}\cdot\mathbf{r}), \tag{6}$$

and

$$\xi_B(\mathbf{r}) = \xi_{B0} + \sum_{\mathbf{q}\neq\mathbf{0}} \hat{\xi}_{B,\mathbf{q}} \exp(i\mathbf{q}\cdot\mathbf{r}), \tag{7}$$

where, without any loss of generality, one can select a coordinate system with $\xi_{A0}=0$.

For the two planar surfaces formed by components A and B, the Hamiltonian can be written as the sum of energy costs of small scale fluctuations about the reference planar surface. This is identical to the single-surface CWM, but applied to two surfaces, and can be written as

$$H_{AB,0} \simeq \frac{\gamma_{A0}}{2}\int \mathbf{dr}|\nabla\xi_A(\mathbf{r})|^2 + \frac{\gamma_{B0}}{2}\int \mathbf{dr}|\nabla\xi_B(\mathbf{r})|^2. \tag{8}$$

The capillary waves acting at the two surfaces should not be independent in general. Atomic sites at each surface forming the interface interact with each other and these interactions should also be included in the Hamiltonian. Consider a site on surface A at $(\mathbf{r}_A,\xi_A(\mathbf{r}_A))$ interacting with a site on surface B at $(\mathbf{r}_B,\xi_B(\mathbf{r}_B))$ via a pair potential $U_{AB}[\mathbf{r}_B-\mathbf{r}_A,\xi_B(\mathbf{r}_B)-\xi_A(\mathbf{r}_A)]$. Since, on average, the two surfaces are planar and density variations in the plane of the interface are usually assumed to be negligible [1], the interaction energy is approximately a function of the interplanar separation.

In view of the Gaussian fluctuations of the interface observed for various interfaces [13,29], we approximate the coupling between the two surfaces per unit area to lowest order as harmonic about a mean separation L_0,

$$U_{AB} \simeq \frac{K_{AB}}{2}(\xi_B-\xi_A-L_0)^2, \tag{9}$$

and the harmonic coupling constant K_{AB} is a positive quantity.

The Hamiltonian for the coupled interface can now be written as the sum of the independent surface Hamiltonian, $H_{AB,0}$ [Eq. (8)], and the coupling between the two surfaces, U_{AB} [Eq. (9)] integrated over the surface.

$$H_{AB} \simeq \frac{\gamma_{A0}}{2}\int \mathbf{dr}|\nabla\xi_A(\mathbf{r})|^2 + \frac{\gamma_{B0}}{2}\int \mathbf{dr}|\nabla\xi_B(\mathbf{r})|^2 + \frac{K_{AB}}{2}\int \mathbf{dr}[\xi_B(\mathbf{r})-\xi_A(\mathbf{r})-L_0]^2, \tag{10}$$

where ∇ is the 2D gradient as defined in Sec. II A.

Using Eqs. (6), (7), and (10), writing the complex Fourier coefficients $\hat{\xi}_{A,\mathbf{q}}=\alpha_{A,\mathbf{q}}+i\beta_{A,\mathbf{q}}$, $\hat{\xi}_{B,\mathbf{q}}=\alpha_{B,\mathbf{q}}+i\beta_{B,\mathbf{q}}$, the Hamiltonian can be rewritten as

$$H_{AB} = \frac{L^2}{2}\sum_{\mathbf{q}\neq\mathbf{0}}\{\gamma_A q^2|\hat{\xi}_{A,\mathbf{q}}|^2 + \gamma_B q^2|\hat{\xi}_{B,\mathbf{q}}|^2 + K_{AB}[(\alpha_{B,\mathbf{q}}-\alpha_{A,\mathbf{q}})^2 + (\beta_{B,\mathbf{q}}-\beta^2_{A,\mathbf{q}})^2]\} + \frac{K_{AB}}{2}L^2(\xi_{B0}-L_0)^2. \tag{11}$$

Using fluctuation theory, the probability of finding an interfacial configuration with Fourier coefficient $\hat{\xi}_{A,\mathbf{q}}$ in the range $\{\hat{\xi}_{A,\mathbf{q}},\hat{\xi}_{A,\mathbf{q}}+d\hat{\xi}_{A,\mathbf{q}}\}$ for all $\mathbf{q}$ and likewise for B, is $\{\Pi_{\mathbf{q}}d\hat{\xi}_{A,\mathbf{q}}d\hat{\xi}_{B,\mathbf{q}}\}c_1\exp(-\beta H_{CW})$, where c_1 is a normalization constant. With the Hamiltonian known, it is straightforward to utilize fluctuation theory and Eq. (11) to obtain expressions for $\langle\alpha^2_{A,\mathbf{q}}\rangle$, $\langle\beta^2_{A,\mathbf{q}}\rangle$, $\langle\alpha_{A,\mathbf{q}}\beta_{A,\mathbf{q}}\rangle$, and likewise for the B surface. The CW amplitudes are then found to be

$$\langle|\hat{\xi}_{A,\mathbf{q}}|^2\rangle = \frac{1}{(\gamma_{A0}+\gamma_{B0})\beta L^2}\left[\frac{1}{q^2}+\frac{r_{BA}}{\frac{K_{AB}}{\gamma_h}+q^2}\right], \tag{12}$$

and

$$\langle|\hat{\xi}_{B,\mathbf{q}}|^2\rangle = \frac{1}{(\gamma_{A0}+\gamma_{B0})\beta L^2}\left[\frac{1}{q^2}+\frac{r_{AB}}{\frac{K_{AB}}{\gamma_h}+q^2}\right], \tag{13}$$

where γ_h is the harmonic mean of γ_{A0} and γ_{B0}, $r_{BA}=\gamma_{B0}/\gamma_{A0}$ and $r_{AB}=1/r_{BA}$. Note that in the limit $K_{AB}\to 0$, the

CW amplitudes for each surface are identical to the single-surface approximation [Eq. (5)] as expected. It can be verified that the equipartition theorem holds for each surface.

The widths of the two surfaces due to CW broadening can be written as $\sigma_A^2=\Sigma_{\mathbf{q}\neq\mathbf{0}}\langle|\hat{\xi}_{A,\mathbf{q}}^2|\rangle$ and $\sigma_B^2=\Sigma_{\mathbf{q}\neq\mathbf{0}}\langle|\hat{\xi}_{B,\mathbf{q}}^2|\rangle$. In the continuum limit, the sum over q in the expression for width can be replaced by an integral, $\Sigma_{\mathbf{q}}\rightarrow(\frac{L}{2\pi})^2\int 2\pi q dq$, with the limits of integration being $\frac{2\pi}{L}$ and $\frac{2\pi}{L_m}$. The L_m values for the two components of the liquid-liquid interface should be equal since they are in equilibrium. Performing the integration, the CW broadened widths for the two surfaces are

$$\sigma_A^2=\frac{1}{4\pi\beta\gamma_{AB}^0}\left\{\ln\left(\frac{L}{L_m}\right)+\frac{r_{BA}}{2}\ln\left(\frac{\frac{K_{AB}}{\gamma_h}+\frac{4\pi^2}{L_m^2}}{\frac{K_{AB}}{\gamma_h}+\frac{4\pi^2}{L^2}}\right)\right\}, \quad (14)$$

and

$$\sigma_B^2=\frac{1}{4\pi\beta\gamma_{AB}^0}\left\{\ln\left(\frac{L}{L_m}\right)+\frac{r_{AB}}{2}\ln\left(\frac{\frac{K_{AB}}{\gamma_h}+\frac{4\pi^2}{L_m^2}}{\frac{K_{AB}}{\gamma_h}+\frac{4\pi^2}{L^2}}\right)\right\}, \quad (15)$$

where $\gamma_{AB}^0=\frac{1}{2}(\gamma_{A0}+\gamma_{B0})$. The lower limit of integration over q cannot be extended to zero just as for the liquid-vapor CWM.

There is an additional contribution to the width of surface B arising from fluctuations in ξ_{B0} due to coupling with surface A, but it exists even in the absence of capillary waves. Note that σ_B^2 is defined with respect to the center of the surface, ξ_{B0}. Defining $\sigma_d^2=2/(\beta K_{AB}L^2)$ and $t_0=L_0/\sigma_d$, the ξ_{B0} dependent term in the Hamiltonian allows us to obtain expressions for the mean and mean of squares of ξ_{B0}.

$$\langle\xi_{B0}\rangle=L_0+\frac{\sigma_d}{\sqrt{\pi}}\left[\frac{\exp(-t_0^2)}{1-\mathrm{erf}(t_0)}\right], \quad (16)$$

and

$$\langle\xi_{B0}^2\rangle=L_0^2+\frac{1}{2}\sigma_d^2+\frac{L_0\sigma_d}{\sqrt{\pi}}\left[\frac{\exp(-t_0^2)}{1-\mathrm{erf}(t_0)}\right]. \quad (17)$$

The width σ_{B0}^2 can be obtained as the variance. For $L\rightarrow\infty$, $\sigma_d\rightarrow 0$, $\langle\xi_{B0}\rangle\rightarrow L_0$, and $\langle\xi_{B0}^2\rangle\rightarrow L_0^2$. Within the harmonic coupling model for a given liquid-liquid interface in the thermodynamic limit, separation between the centers of the two surfaces tends to a constant value.

Having identified the different contributions to the width of surfaces A and B, we now obtain expressions for the distribution of surface positions. For the special case $\gamma_{A,0}\simeq\gamma_{B0}=\gamma_0$, expected for an equilibrium interface, the distribution of surface positions can be shown to be

$$P(\xi_A)=\frac{1}{\sqrt{2\pi\sigma_A^2}}\exp\left[\frac{-\xi_A^2}{2\sigma_A^2}\right], \quad (18)$$

and

$$P(\xi_B)=\frac{1}{\sqrt{2\pi(\sigma_B^2+\sigma_d^2)}}\exp\left[\frac{-(\xi_B-L_0)^2}{2(\sigma_B^2+\sigma_d^2)}\right]\chi(\xi_B), \quad (19)$$

where $\chi(\xi_B)$ is defined as

$$\chi(\xi_B)=\frac{1-\mathrm{erf}\left[\frac{L_0\sigma_B/\sigma_d+\xi_B\sigma_d/\sigma_B}{\sqrt{2\sigma_B^2+\sigma_d^2}}\right]}{1-\mathrm{erf}\left[\frac{L_0}{\sqrt{2}\sigma_d}\right]}, \quad (20)$$

and the variance obtained for each surface given by Eqs. (14) and (15). In the limit of large L, $\sigma_d\rightarrow 0$ and one obtains $\chi(\xi_B)=1$. The distribution of positions for the right surface B then becomes

$$P(\xi_B)\sim\frac{1}{\sqrt{2\pi\sigma_B^2}}\exp\left[\frac{-(\xi_B-L_0)^2}{2\sigma_B^2}\right]. \quad (21)$$

C. Model 2: Coupled surfaces and interactions with bulk

A shortcoming of model 1 and of the CWM is the divergence of the capillary-wave contribution to surface width in the thermodynamic limit. While it is possible for these widths to diverge in the case of isolated surfaces, a divergent width is unphysical unless the bulk component attached to the surface can be compressed indefinitely in order to support these divergent surface fluctuations. The presence of a bulk component next to the surface is therefore expected to damp the surface fluctuations. A second shortcoming of model 1 is the limitation of its applicability to length scales larger than some unknown small value L_m. While the notion of a surface becomes suspect at small length scales, it would be useful to extend the range of applicability of model 1 to all length scales.

In order to improve the model, we start by incorporating the interaction of the surface layer with the attached bulk components. As shown in our previous paper [12], an interface within the "convolution approximation" [30] can be represented as an intrinsic profile attached to a planar surface which fluctuates due to the action of capillary waves. The surface can be thought of as moving in a mean field due to the intrinsic profile. To lowest order, this interaction can be assumed to be harmonic in fluctuations from planarity. We therefore add a correction term to the surface Hamiltonian for model 1 to account for these surface-bulk interactions as

$$H_{c1}=\frac{K_{AA}}{2}\int\mathbf{dr}[\xi_A(\mathbf{r})-\xi_{A0}]^2+\frac{K_{BB}}{2}\int\mathbf{dr}[\xi_B(\mathbf{r})-\xi_{B0}]^2, \quad (22)$$

where K_{AA} and K_{BB} are the harmonic surface-bulk coupling constants for the A and B surfaces, respectively. Interactions between the bulk phase of one component with the surface of the other are assumed to be negligible.

Introducing the Fourier expansion for both surfaces into Eq. (22), and adding the surface-bulk contribution to the coupled surface Hamiltonian, Eq. (11), the total Hamiltonian becomes

$$H_{AB} = \frac{K_{AB}}{2} L^2 \{\xi_{B0} - L_0\}^2 + \frac{L^2}{2} \sum_{\mathbf{q}\neq\mathbf{0}} [(\gamma_{A0} q^2 + K_{AA}) |\hat{\xi}_{A,\mathbf{q}}|^2 + (\gamma_{B0} q^2 + K_{BB}) |\hat{\xi}_{B,\mathbf{q}}|^2 + K_{AB} \{(\alpha_{B,\mathbf{q}} - \alpha_{A,\mathbf{q}})^2 + (\beta_{B,\mathbf{q}} - \beta_{A,\mathbf{q}})^2\}]. \quad (23)$$

Defining $K_1 = K_{BB} + K_{AB}$, $K_2 = K_{AA} + K_{AB}$, and $K_3 = K_1 K_2 - K_{AB}^2$, the capillary-wave amplitudes for the two surfaces can be shown to be

$$\langle |\hat{\xi}_{A,\mathbf{q}}|^2 \rangle = \frac{1}{\beta L^2} \frac{K_1 + \gamma_{B0} q^2}{K_3 + q^2(\gamma_{A0} K_1 + \gamma_{B0} K_2) + \gamma_{A0} \gamma_{B0} q^4}, \quad (24)$$

and

$$\langle |\hat{\xi}_{B,\mathbf{q}}|^2 \rangle = \frac{1}{\beta L^2} \frac{K_2 + \gamma_{A0} q^2}{K_3 + q^2(\gamma_{A0} K_1 + \gamma_{B0} K_2) + \gamma_{A0} \gamma_{B0} q^4}. \quad (25)$$

It should be noted that unlike the CWM and model 1, the q^{-2} term in the CW amplitude is lost due to the surface-bulk coupling. Setting $K_{AA} = K_{BB} = 0$, the q^{-2} term is recovered since $K_3 = 0$. The large-L divergence of CW broadened width in those two models came from the term resulting from the integral of the q^{-2} term. One therefore expects the current model to have a finite width in the thermodynamic limit.

The width of the interface has two contributions just as in model 1. Fluctuations in ξ_{B0} lead to a width identical to that in model 1. However, the CW contributions are different. For surface A,

$$\sigma_A^2 = \frac{1}{8\pi\beta\gamma_{A0}} \left\{ \ln\left[\frac{K_3 + a_1/L_m^2 + a_2/L_m^4}{K_3 + a_1/L^2 + a_2/L^4} \right] + b_1 \ln\left[\left(\frac{b_2 + L_m^2}{b_3 + L_m^2} \right) \left(\frac{b_3 + L^2}{b_2 + L^2} \right) \right] \right\}, \quad (26)$$

where

$$a_1 = 4\pi^2 (K_1 \gamma_{A0} + K_2 \gamma_{B0}),$$

$$a_2 = 16\pi^4 \gamma_{A0} \gamma_{B0},$$

$$b_1 = \frac{(K_1 \gamma_{A0} - K_2 \gamma_{B0})}{\sqrt{(K_1 \gamma_{A0} - K_2 \gamma_{B0})^2 + 4K_{AB}^2 \gamma_{A0} \gamma_{B0}}},$$

$$b_2 = 4\pi^2/(c_1 - c_2),$$

$$b_3 = 4\pi^2/(c_1 + c_2),$$

$$c_1^2 = \frac{(K_1 \gamma_{A0} - K_2 \gamma_{B0})}{(4\gamma_{A0} \gamma_{B0})},$$

$$c_2 = \frac{(K_1 \gamma_{A0} + K_2 \gamma_{B0})}{(2\gamma_{A0} \gamma_{B0})},$$

and the expression for σ_B^2 can be obtained from Eq. (26) by replacing γ_{A0} in the denominator of the prefactor by γ_{B0} and replacing b_1 by $-b_1$.

While this expression is more complicated than the CWM, in the limit $L \to \infty$, the CW broadened width reaches a constant value instead of the usual CWM divergence. Introduction of surface-bulk coupling has therefore prevented the diverging interfacial width in the thermodynamic limit. On the other hand, the divergence of the width as $L_m \to 0$ still survives this modification. This divergence arises from the first term in the expression for the width only; the second term is finite for both $L_m \to 0$ and $L \to \infty$. This model therefore requires a large q cutoff and consequently, a small length scale above which it can be applied.

D. Model 3: Coupled surfaces, interactions with bulk and curvature corrections

A more complete description of the surface Hamiltonian should account for surface curvature effects on surface fluctuations. These corrections can be included by adding the term

$$H_{c2} = \frac{1}{2} \int \mathbf{dr} \{\kappa_A [\nabla^2 \xi_A]^2 + \kappa_B [\nabla^2 \xi_B]^2\} \quad (27)$$

to the coupled CW Hamiltonian [Eq. (10)], where κ_A and κ_B are the bending rigidities of surfaces A and B, respectively, and $\nabla^2 = \partial^2/\partial x^2 + \partial^2/\partial y^2$ [20,26]. The two bending rigidities are assumed to have different magnitudes here. Introducing the Fourier expansion of the two surfaces, H_{c2} can be rewritten as

$$H_{c2} = \frac{L^2}{2} \sum_{\mathbf{q}\neq\mathbf{0}} \{\kappa_A q^4 |\hat{\xi}_{A,\mathbf{q}}|^2 + \kappa_B q^4 |\hat{\xi}_{B,\mathbf{q}}|^2\}. \quad (28)$$

Defining $\Gamma_A(q) = \gamma_{A0} + \kappa_A q^2$ and $\Gamma_B(q) = \gamma_{B0} + \kappa_B q^2$, the Hamiltonian for this model has the same form as the Hamiltonian for model 2 [Eq. (23)] with γ_{A0} replaced by Γ_A (implicit q dependence) and likewise for γ_{B0}.

Since the only difference between this model and model 2 is the q-dependent surface tension for each surface, we can write the expression for the CW amplitudes by analogy as

$$\langle |\hat{\xi}_{A,\mathbf{q}}|^2 \rangle = \frac{1}{\beta L^2} \frac{K_1 + \Gamma_B q^2}{K_3 + q^2(\Gamma_A K_1 + \Gamma_B K_2) + \Gamma_A \Gamma_B q^4}, \quad (29)$$

and

$$\langle |\hat{\xi}_{B,\mathbf{q}}|^2 \rangle = \frac{1}{\beta L^2} \frac{K_2 + \Gamma_A q^2}{K_3 + q^2(\Gamma_A K_1 + \Gamma_B K_2) + \Gamma_A \Gamma_B q^4}. \quad (30)$$

For the special case of $\gamma_{A0} \sim \gamma_{B0} = \gamma$ and $\kappa_A \sim \kappa_B = \kappa$, it can be shown that the surface widths do not diverge in the limit $L_m \to 0$ and one obtains the following expressions for the width of surface B in this limit:

$$\sigma_B^2 = \frac{a_1}{\beta} \ln\left(\frac{1 + L^2 c_2}{1 + L^2 c_1} \right) + \frac{a_2}{\beta} \ln\left(\frac{1 + L^2 c_4}{1 + L^2 c_3} \right), \quad (31)$$

where

$$a = (K_1 + K_2)/2,$$

$$b = \frac{1}{2} \sqrt{(K_1 - K_2)^2 + 4K_{AB}^2},$$

$$a_1 = \frac{(a+b-K_1)}{(16\pi b\kappa f_2)},$$

$$a_2 = \frac{(b-a+K_1)}{(16\pi b\kappa f_2)},$$

$$f_1 = \gamma/2\kappa,$$

$$f_2 = \sqrt{\gamma^2/4\kappa^2 - (a+b)/\kappa},$$

$$f_3 = \sqrt{\gamma^2/4\kappa^2 - (a-b)/\kappa},$$

$$c_1 = (f_1 - f_2)/(4\pi^2),$$

$$c_2 = (f_1 + f_2)/(4\pi^2),$$

$$c_3 = (f_1 - f_3)/(4\pi^2),$$

and

$$c_4 = (f_1 + f_4)/(4\pi^2).$$

This expression for σ_B^2 is valid for $\gamma^2 > 4\kappa(a+b)$. The corresponding equation for σ_A^2 can be obtained by replacing K_1 with K_2 in a_1 and a_2. The surface widths do not diverge in the thermodynamic limit and reach a finite value unlike model 2. For comparison it should be pointed out that the addition of curvature corrections to model 1 prevents the divergence in the limit $L_m \to 0$ but not the divergence for $L \to \infty$. A disadvantage of this model is the introduction of additional parameters and the resulting complicated functional forms.

E. Capillary-wave contribution to surface tension

As mentioned in Sec. II A, surface fluctuations of the liquid-vapor interface were partitioned into contributions with wave numbers larger than $2\pi/L_m$ (leading to the bare surface tension which occurs in the expression for width) and contributions from wave number smaller than $2\pi/L_m$ (the capillary waves). Kayser [16] obtained the analytic form of the CW contribution to the surface tension which allows for a calculation of the total surface tension that can be compared with the macroscopic surface tension. We adapt Kayser's analysis for the liquid-vapor interface to the liquid-liquid interface.

The starting point for this derivation is the total free energy F_{tot} of formation for the interface consisting of two surfaces A and B each with surface area S. Let F_A and F_B be the free energies of formation of surfaces A and B where fluctuations with a wave number larger than $2\pi/L_m$ have been unfrozen on the surface. By definition, the bare surface tensions are related to these free energies via $\gamma_A = \partial F_A/\partial S$ (and an identical relation for γ_B). The contribution of the capillary waves with a wave number smaller than $2\pi/L_m$ are unfrozen upon these two surfaces and the free energy contribution due to these fluctuations, F_{CW}, needs to be included for comparison with the macroscopic surface tension. The total free energy is then the sum of these three contributions and one obtains $F_{\text{tot}} = F_A + F_B + F_{CW}$. Since the total surface area of the interface assuming small deviations from planarity is $2S$, the total surface tension of the interface, γ_{AB}, after taking the partial derivative with respect to the area is

$$\gamma_{AB} = \frac{\partial F_{\text{tot}}}{\partial(2S)} = \frac{\gamma_{A,0} + \gamma_{B,0}}{2} + \gamma_{CW}, \tag{32}$$

where $\gamma_{CW} = \partial F_{CW}/\partial(2S)$.

Since L_m is defined as the smallest applicable length scale, partition the two surfaces forming the interface so that the system is partitioned into columns with an area of cross section $L_m \times L_m$. The continuous surface can then be represented instead by the set of heights $\{\xi(\mathbf{r}_{i,X})\}$, where $X = A, B$ and $\mathbf{r}_{i,X}$ is the position of the ith column of surface X in the (x,y) plane. By construction, the total number of columns is identical to the number of variables, i.e., the number of capillary waves that have been unfrozen on the surface.

According to Weeks [7], the CW Hamiltonian is obtained by integrating out bulk density fluctuations on scales smaller than the bulk correlation length and the surface width at these small length scales is proportional to the bulk correlation length. So the fluctuations in the height of the two surfaces forming the liquid-liquid interface can be considered as arising from fluctuations in the number $N_{i,A}$ of coherent density fluctuations of size equal to the bulk correlation length in column i for component A. Identifying $\bar{N}_A$ as the average number of "blobs" [16,31] and $l_{0,A}$ as the bulk correlation length for component A, the height of column i can be written as

$$\xi(\mathbf{r}_{i,A}) = \xi_{A,0} + (N_{i,A} - \bar{N}_A)\frac{l_{0,A}^3}{L_m^2}, \tag{33}$$

and a similar expression for the height of column i of component B with the subscript A replaced by B.

For this discrete representation of the system, the partition function can be written as

$$Z(\beta) = \prod_i \int d\xi_{i,A} c_A \int d\xi_{i,B} c_B \exp(-\beta H_{CW}), \tag{34}$$

where $d\xi_{i,A}$ and $d\xi_{i,B}$ are the height fluctuations of the ith column of components A and B, and c_A and c_B are constants with dimensions of inverse length that have to be determined. Making the transformation from $\xi(\mathbf{r}_{i,A})$ to $N_{i,A} - \bar{N}_A$ via Eq. (33) leads to an expression for Z in terms of the dimensionless fluctuation variable $(N_{i,A} - \bar{N}_A)$. Setting the constant of proportionality equal to unity [16,31] leads to $c_A = L_m^2/l_{0,A}^3$ and $c_B = L_m^2/l_{0,B}^3$. Substituting these expressions for c_A and c_B into Eq. (34) leads to

$$Z(\beta) = \prod_i \frac{L_m^4}{l_{0,A}^3 l_{0,B}^3} \int d\xi_{i,A} \int d\xi_{i,B} \exp(-\beta H_{CW}). \tag{35}$$

As evident from the description of models 1–3, the Hamiltonian is simplified when the Fourier representation of the surface [Eqs. (6) and (7)] is introduced. The Jacobian of the transformation from $\xi_{i,A}$ to $\hat{\xi}_{A,\mathbf{q}}$ is $\sqrt{A/L_m^2}$ [16] and the trans-

formation from $\{\hat{\xi}_{A,\mathbf{q}}, \hat{\xi}_{A,-q}\}$ to $(\alpha_{A,q}, \beta_{A,q})$ leads to an additional factor of 2. After these two transformations, the CW partition function takes the form

$$Z(\beta) = \left\{ \frac{2L_m^2 A}{l_{0,A}^3 l_{0,B}^3} \right\}^2 \prod_{\mathbf{q}\neq\mathbf{0}} \int d\alpha_{A,q} d\beta_{A,q} \int d\alpha_{B,q} d\beta_{B,q} \times \exp(-\beta H_{CW}). \tag{36}$$

Formal expressions for the CW contribution to free energy are obtained here for model 2 by introducing H_{CW} from Eq. (23) into Eq. (36) and using the relation $Z(\beta)=\exp(-\beta F_{CW})$. The $\mathbf{q}=0$ term in the Hamiltonian is ignored here since it does not correspond to capillary fluctuations of interest. The resulting expression for the free energy is

$$\beta F_{CW} = \sum_{\mathbf{q}\neq\mathbf{0}} \ln\{G_1 f(q)\}, \tag{37}$$

where

$$f(q) = K_3 + (\gamma_{A0}K_1 + \gamma_{B0}K_2)q^2 + \gamma_{A0}\gamma_{B0}q^4, \tag{38}$$

and

$$G_1 = \left\{ \frac{l_{0,A}^3 l_{0,B}^3 \beta}{2\pi L_m^2} \right\}^2. \tag{39}$$

In the continuum limit, the sum over wave vectors is replaced by the integral over $\mathbf{q}$ and the expression for the CW contribution to the surface tension, $\gamma_{CW}=\partial F_{CW}/\partial(2S)$, is

$$\beta\gamma_{CW} = -\frac{1}{8}\{q_{\max}^2 - q_{\min}^2\} + \frac{q_{\max}^2}{16}\ln[G_1 f(q_{\max})] - \frac{q_{\min}^2}{16}\ln[G_1 f(q_{\min})] + \frac{g_-}{16}\ln\left\{\frac{q_{\max}^2 + g_-}{q_{\min}^2 + g_-}\right\} + \frac{g_+}{16}\ln\left\{\frac{q_{\max}^2 + g_+}{q_{\min}^2 + g_+}\right\}, \tag{40}$$

where

$$g_\pm = \frac{\gamma_{A0}K_1 + \gamma_{B0}K_2}{\gamma_{A0}\gamma_{B0}} \pm \sqrt{\frac{K_{AB}^2}{\gamma_{A0}\gamma_{B0}} + \left(\frac{\gamma_{A0}K_1 - \gamma_{B0}K_2}{2\gamma_{A0}\gamma_{B0}}\right)^2}. \tag{41}$$

With the three models for liquid-liquid interfaces and the CW contribution to surface tension available, in the following we present our simulation method and test the model predictions based on the configurations obtained.

III. SIMULATION DETAILS

Molecular dynamics (MD) simulations are carried out for two series of water-hydrocarbon interfaces. In series 1, the hydrocarbon chain length is kept constant for *n*-pentane (P), 2-methyl pentane (2MP), and 2,2,4-trimethyl pentane (TMP). For series 2, the molecular mass of the hydrocarbon component of the interface is held fixed for *n*-octane (O), 2-methyl heptane (2MH), and 2,2,4-trimethyl pentane (TMP).

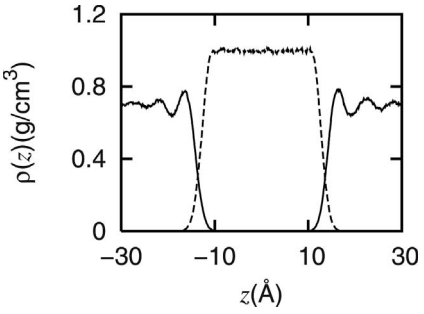

FIG. 1. Density profiles for the water (dashed line)-TMP (solid line) system.

The simulation protocol is summarized here and details can be found elsewhere [12]. The force fields adopted are simple point charge/extended (SPC/E) [32] for water and united atom optimized potential for liquid simulation (OPLS) for hydrocarbon molecules [33,34]. The usual Lorentz-Berthelot combination rules [35] were used to describe Lennard-Jones interactions between unlike sites. Electrostatic interactions were handled with Wolf's method [36–38]. Temperature and pressure were kept constant at 298.15 K and 1 atm using Berendsen's thermostat and barostat [39]. Periodic boundary conditions were applied along all three Cartesian directions.

The number of water (W) molecules is kept fixed at 586 and the water layer is sandwiched between two hydrocarbon (H) layers, each containing an equal number of molecules initially. The number of hydrocarbon molecules in each layer was 91 for *n*-pentane, 79 for 2-methyl pentane, and 64 for all other hydrocarbons. This ensures an equal area of cross section of the interface for all systems. After an initial equilibration run of 250 ps, simulations are continued for an additional 1 ns and 50 000 configurations are saved at intervals of 20 fs. The density profile for the equilibrated water-TMP system indicative of the simulation setup is shown in Fig. 1.

Pressure and surface tension values were obtained using the virial [Eq. (42)], where $p_{\alpha\alpha}$ is the instantaneous (α,α) component of the pressure tensor and L_z is the instantaneous size of the simulation box in the z direction. Surface tension values so obtained are listed in Table I and differ from experimental values [40,41] which are typically in the 50–60 mN/m range. The values obtained from MD simulation depend on the force field and possibly also on the simulation protocol. For hydrocarbons, they are usually underestimated for the united atom OPLS force field [15,42].

$$\gamma = \frac{1}{2}\left\langle \left[p_{zz} - \frac{1}{2}(p_{xx} + p_{yy}) \right] L_z \right\rangle. \tag{42}$$

In order to test the predictions of the CW models for liquid-liquid interfaces, a surface needs to be identified. Instead of using the usual Gibbs definition of a surface, we seek an atomic-level representation. By definition, a site on the surface of one liquid component forming the interface is closer to the second liquid component than a site away from it. A simple implementation of this idea is utilized to identify the surface water sites with respect to the hydrocarbon layer and

TABLE I. Characteristic properties of the water (B)-hydrocarbon (A) interface for different hydrocarbons: The columns represent the hydrocarbon name, mean separation between centers of the two surfaces, L_0 (Å), average (over A and B surfaces) squared width due to CW fluctuations, σ^2 (Å^2), average squared width due to bulk contributions to surface fluctuations, σ_0^2 (Å^2), L_m (Å^2), AA harmonic coupling constant, $K_{AA}(k_bT$ Å$^{-4})$ ($K_{AA} \simeq K_{BB}$), AB harmonic coupling constant, $K_{AB}(k_bT$ Å$^{-4})$, surface tension based on fit to model 2, γ_{fit} (10^{-3} N/m), squared width due to capillary waves as predicted by model 2, σ_A^2 (Å^2), correlation length value for the hydrocarbon, $l_{0,A}$ (Å), CW contribution to the surface tension, γ_{CW} (10^{-3} N/m), total CW contribution to the surface tension predicted by model 2, γ_p (10^{-3} N/m), surface tension from simulation, γ_{sim} (10^{-3} N/m).

Hydrocarbon	L_0	σ_A^2	σ_0^2	L_m	K_{AA}	K_{AB}	γ_{fit}	σ_p^2	$l_{0,A}$	γ_{CW}	γ_p	γ_{sim}
P	2.87	2.38	0.06	8.14	0.00119	0.0012	34.23	2.45	5.33	−5.11	29.12	30.96
2MP	2.92	2.20	0.06	8.19	0.00186	0.0014	36.62	2.49	5.21	−5.64	30.98	30.26
TMP	2.98	2.13	0.07	8.29	0.00078	0.0021	37.49	2.18	5.76	−2.651	34.84	34.37
2MH	2.98	2.12	0.06	8.19	0.00081	0.0027	36.74	2.22	5.51	−3.304	33.44	34.03
O	2.99	2.19	0.06	8.08	0.00003	0.0034	36.65	2.28	5.53	−3.056	33.59	33.42

the hydrocarbon surface sites with respect to the water layer. Details of this surface identification can be found elsewhere [12].

IV. SURFACE ANALYSIS

With the surface sites available, their distributions and fluctuations can be analyzed and parameters required for testing predictions of the three models obtained from this analysis. In Sec. IV A, the two length scales L_0 and L_m are estimated from the distribution of surface sites and surface or bulk contributions to the width. The Fourier transformed height-height correlation function, i.e., the CW spectrum, is extracted from the positions of the surface sites. The large q part of the spectrum is dominated by bulklike contributions, which makes fitting the large q unreliable. Consequently, the CW spectrum is fit in the range $q \in [2\pi/L, 2\pi/L_m]$ to the functional forms predicted by model 2 and the model parameters K_{AB}, K_{AA}, and K_{BB}, as well as surface tension γ_{AB} are obtained from the fit. These calculations are presented in Sec. IV B and the predicted value of the CW broadened width based on these parameters compared with the simulated value. For the simulation setup used, there are two water-hydrocarbon interfaces and all data is averaged over the two surfaces for analysis.

A. Obtaining L_m and L_0

A key characteristic of the surface is the distribution of surface positions. Identifying the set of surface sites with a statistical sampling of the possible surface positions, the distribution of surface positions can be constructed from the simulation data. All three models presented in Sec. II lead to a Gaussian distribution of surface sites with the left surface of the interface centered at the origin. The relevant expressions are Eq. (18) and Eq. (19) or (21) from which one can obtain σ_A^2, σ_B^2, L_0, and σ_d^2, where A and B correspond to the hydrocarbon and water surfaces, respectively. In the limit of large L, σ_d^2 is a small number and a fit to the distribution functions might not be the best procedure for obtaining its value due to differences in the order of magnitude of σ_d^2 and σ_A^2 or σ_B^2. Since σ_A^2 is by definition the width of the surface centered at the origin, it can be obtained from a fit to the distribution of surface sites forming the lower surface with the center of the distribution set as the origin, regardless of the distribution of surface site positions for the right surface. With the upper surface centered at the origin, the distribution of surface positions can also be fit to obtain σ_B^2, independent of the distribution of sites forming the left surface.

The distribution of surface sites for the hydrocarbon and water surfaces forming the two interfaces is shown in Fig. 2. Fits of the distribution of surface sites to Eqs. (18) and (19) are excellent and validate the predicted form from the model. The values for σ_A^2, σ_B^2, and L_0 obtained from these fits are listed in Table I.

Turning to L_m, since it affects the surface width logarithmically [Eqs. (4), (14), and (15)], knowing its order of magnitude should be sufficient for making reasonable estimates of surface width. The only consensus on its physical interpretation is that outside the range of applicability of the CWM ($L < L_m$), its predictions should break down, which in turn suggests a simple procedure for identification of L_m. Following Weeks [7], we partition the (x,y) plane into grids of size L/n_g, where n_g is selected to lie between 1 (the full interface) and 7 (roughly the LJ diameter of the oxygen atom for SPC/E water). This approximately allows us to study the interface for different values of L.

Next, consider the raw distribution of surface positions for the hydrocarbon surface (A) as obtained from the simulation. As suggested by the Fourier representation of the in-

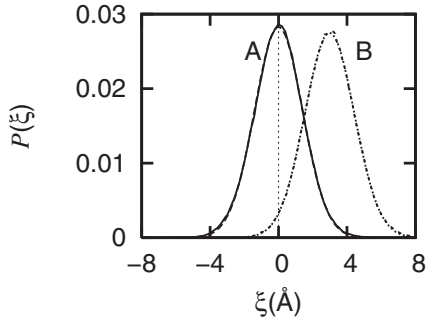

FIG. 2. The distribution of surface sites for water (B, short dashes) and TMP (A, solid line). Also shown are the fits of distribution of surface sites to Eqs. (18) and (19) for the water (dots) and TMP (long dashes) surfaces.

stantaneous surface [Eqs. (6) and (7)], surface positions are centered about ξ_{A0} with additional contributions $\hat{\xi}_{A,\mathbf{q}}$ arising due to different wavelength capillary waves. The center of the distribution can differ for different manifestations of the surface due to bulk fluctuations and a distribution $P_c(\xi_{A0})$ of the locations of its centers ξ_{A0} can be constructed. The width of this distribution would give the bulk contribution to surface width of A. With respect to ξ_{A0}, the distribution of surface positions, $P_{\mathrm{CW}}(z-\xi_{A0})$, would be free of bulk contributions and represents the CW contribution to the surface broadening only. Assuming that the bulk and capillary contributions to surface positions are uncorrelated, the distribution of surface positions for surface A, $P_A(z)$, can be thought of as the convolution, $P_A(z)=\int d\xi_{A0} P_c(\xi_{A0}) P_{\mathrm{CW}}(z-\xi_{A0})$. The width of $P_{CW}(z-\xi_{A0})$ is the usual CW contribution to surface width of A for $n_g=1$.

For each grid corresponding to a selected value of n_g, the center of mass of the water (B) layer is shifted to zero. With the center of mass of the water column for each grid at $z=0$, the distributions $P_c(n_g,\xi_{A0})$, $P_{CW}(n_g,z-\xi_{A0})$, $P_c(n_g,\xi_{B0})$, and $P_{CW}(n_g,z-\xi_{B0})$ are constructed from the hydrocarbon and water surface sites that belong to a particular grid of size L/n_g. A similar procedure has been reported in the literature [13,14] to study the n_g dependence of $P_A(z)$, although instead of defining a surface layer and setting the origin at zero for each grid, only the extremal molecules or molecular sites in each grid were considered with n_g chosen to give a minimum length scale corresponding to the bulk correlation length.

The distributions $P_c(n_g,\xi_{A0})$ and $P_{CW}(n_g,z-\xi_{A0})$ for the right hydrocarbon surface layer are shown in Figs. 3(a) and 3(b), respectively. The CWM predicts a Gaussian form for $P_{CW}(1,\xi_{A0})$ and that is indeed what we find. In fact, both distributions are well described by a Gaussian functional form for all values of n_g shown. If the breakdown of the CWM occurs at some length scale sampled by these different n_g, it is not possible to identify such a length scale based on $P_{CW}(n_g,z-\xi_{A0})$ since there is no drastic change over the range of n_g probed. The only trend that can be observed is a narrowing of $P_{CW}(n_g,z-\xi_{A0})$ and broadening of $P_c(n_g,\xi_{A0})$ with an increase in n_g. On decreasing n_g one expects the number of surface sites to decrease, which eventually leads to a situation in which a single-surface molecule or site exists in the grid. This limiting case would lead to a delta function distribution of surface positions. The n_g dependence of P_{CW} is consistent with its approach to this limiting case and is similar to the observed trend for a 3D Ising spin system [43].

The bulk contributions to the surface width, $\sigma^2_{A0}(n_g)$ and $\sigma^2_{B0}(n_g)$, and the capillary contributions to the width, $\sigma^2_A(n_g)$ and $\sigma^2_B(n_g)$, are obtained from fits to the distributions for each grid size and its dependence on L/n_g as shown in Fig. 3(c).

Interpreting the breakdown of CWM at L_m as a gradual transition from a length scale at which the surface is well defined and surface fluctuations make the dominant contribution to the total width to a length scale where bulk fluctuations dominate the total width of a surface, L_m can be approximated as the value of L/n_g at which surface and bulk contributions to the width become equal. We therefore estimate L_m by fitting the L/n_g dependence of surface and bulk widths to polynomials and obtaining its value as the point of intersection of the polynomial. To improve statistics we average the widths for the four interfaces before estimating L_m from their L/n_g dependence. The values of L_m so obtained are reported in Table I. A similar behavior for interfacial width vs grid size has been observed for homopolymer surfaces [44] where instead of identifying a surface layer of sites, a Gibbs surface was constructed for each coarse-graining length scale. The value of L_m is of the order of 8 Å, which is not comparable to any estimate used in previous studies although it appears to be approximately equal to twice the equilibrium pair separation between an oxygen and carbon atom.

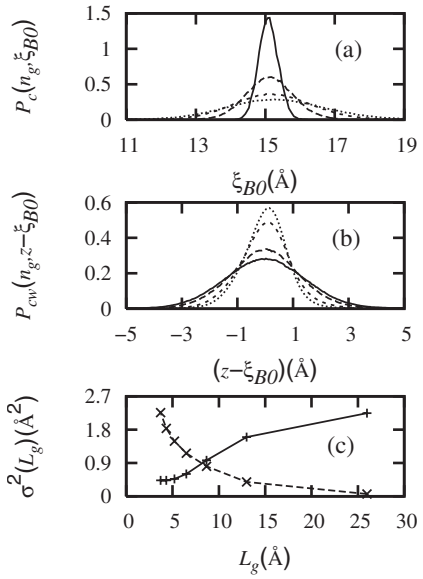

FIG. 3. The effect of coarse graining the surface using grid size $n_g=1$ (solid line), 2 (long dashes), 4 (short dashes), and 6 (dots), on the distribution of surface positions and widths for the water-TMP interface. (a) Probability distribution $P_c(n_g)$ of the center of the distribution, ξ_c, for the right hydrocarbon surface sites, (b) probability distribution $P_{CW}(n_g)$, of surface positions with respect to the center of the distribution for the right hydrocarbon sites, and (c) contributions of the bulk (large dashes) and surface (solid line) fluctuations to the squared width of the hydrocarbon surface layer as a function of coarse graining length scale.

The bulk and capillary contributions to the surface width are presented in Table I. For hydrocarbons in series 1, there is a reduction in the CW width for the hydrocarbon and water surfaces on going from P to TMP. For this series, the chain length is fixed and the effect of branching is to make the molecule more globular. As shown elsewhere [12,45], hydrocarbon molecules at the interface adopt a stacked configuration. For the more globular molecule on going from P to TMP, the energetic cost for surface fluctuations will be higher thereby leading to a larger surface tension and a corresponding smaller CW width as indicated by the data. Numerically, the widths for TMP, 2MP, and 2MH are comparable and indicate the similarity of surface roughness for these interfaces. For series 2, going from O to TMP, the total mass is fixed but the chain length varies. The CW width of

the surface decreases slightly on going from TMP to TMH and increases from TMH to O. It appears that an increase in chain length, from P to O and 2MP to 2MH, leads to a smaller width for the longer hydrocarbon. In addition, an increase in branching appears to decrease the width, thereby increasing the surface tension. The bulk contribution to surface width is negligible and shows no systematic behavior either for series 1 or 2.

B. Surface fluctuations

With an estimate for L_m available based on the procedure adopted in the previous section, the range of wave vectors available to the system is known. A comprehensive test of the different models can be made by comparing their predictions for the q dependence of CW amplitudes within the allowed q range. In the absence of model parameters *a priori*, a fit to the simulated q dependence can give a set of model parameters which could then be used to estimate surface characteristics.

The first step is to calculate the CW spectrum for the two surfaces. The coordinates of the surface sites can be fit to Eqs. (6) and (7) in order to obtain the complex Fourier coefficients $\hat{\xi}_{A,\mathbf{q}}$ and $\hat{\xi}_{B,\mathbf{q}}$ [10,11]. However, this procedure is computationally expensive, particularly for large systems, due to the fitting involved. We therefore adopt an alternative procedure suggested by Stecki [46] to estimate $\hat{\xi}_{A,\mathbf{q}}$. For surface A, the z coordinates of the N_A surface sites are known from the simulation and we define $\hat{\xi}_{A,\mathbf{q}}$ as

$$\hat{\xi}_{A,\mathbf{q}} = \frac{1}{N_A}\sum_{j}^{N_A}(z_{j,A} - \xi_{A0})e^{i\mathbf{q}\cdot\mathbf{r}_{j,A}}, \tag{43}$$

where $z_{j,A}$ is the z coordinate for site j on surface A. In the following we will drop the surface label and refer to it according to the associated bulk phase. With the calculated Fourier coefficients, the modulus of the error in predicted [Eqs. (6) and (7)] and actual z coordinates for all surface sites are estimated. Surface sites that are more than 3 Å from the predicted 2D surface are removed from the list of surface sites. This results in elimination of sites that are far from the center of the distribution of surface sites. The Fourier coefficients are recalculated with the new set of surface sites, and the procedure repeated until no new sites are removed from the remaining set of surface sites.

The CW spectrum, or equivalently, the Fourier transform of the height-height correlation function, $\langle\hat{\xi}_{\mathbf{q}}\hat{\xi}_{-\mathbf{q}}\rangle$, can be calculated numerically from $\hat{\xi}_{\mathbf{q}}$ now. This calculation was performed for the four sets of surface sites and averaged over the two water and hydrocarbon surfaces. The wave-vector dependence for the water surface, averaged over the two water surfaces, is presented in Fig. 4 for series 1 water-hydrocarbon interface. The CW spectrum for the hydrocarbon surface, averaged over the two hydrocarbon surfaces, is presented in Figs. 4(b) and 4(c) for series 1 and 2 interfaces, respectively.

A common feature for both components of the interface is the sharp decrease at large q down to a minimum at approximately $q \sim 2\pi/\sigma$, where $\sigma \sim 3.2$ Å for the oxygen atom and 3.4 Å for the hydrocarbon molecules. This represents the CW fluctuations involving large-scale cooperative motion. Beyond this minimum there is an oscillatory component in the CW spectrum which could arise either from local structure in the plane of the surface or from the contribution of bulk fluctuations to the position of surface sites. If bulk fluctuations, on average, act uniformly for all surface sites and their contribution is removed by setting the center of the distribution of surface sites at the origin, the large-q structure might be indicative of structure in the surface layer. To test the connection between in-plane structure and $\langle|\hat{\xi}_{\mathbf{q}}|^2\rangle$, we calculate the in-plane structure factor $S(q)$, defined as

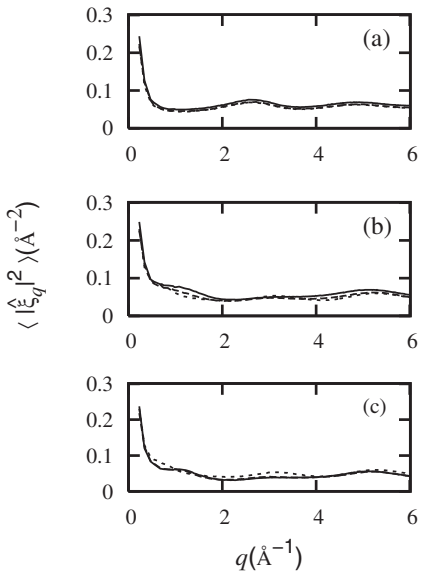

FIG. 4. Capillary-wave spectrum for different surfaces as a function of wave vector q. (a) The water surface for water-P (solid), water-2MP (long dashes), and water-TMP (short dashes). (b) The hydrocarbon surface for water-P (solid), water-2MP (long dashes), and water-TMP (short dashes). (c) The hydrocarbon surface for water-O (solid), water-2MH (long dashes), and water-TMP (short dashes).

$$S(q) = \left\langle \frac{1}{N_p}\sum_{j\neq k}^{N_p} e^{i\mathbf{q}\cdot\mathbf{r}_{jk}} \right\rangle, \tag{44}$$

based on the surface sites at each interface, where N_p is the number of surface sites and $\mathbf{r}_{jk}$ is the in-plane distance vector between the jth and kth surface sites.

For a Lennard-Jones system, Stecki [25] found that the large q part of the CW spectrum was proportional to the structure factor $S(q)$. To check this possibility, we present the structure factor $S(q)$, and the CW spectrum $\langle|\hat{\xi}_{\mathbf{q}}|^2\rangle$, together in Fig. 5 for the water-TMP interface. Since $S(q)\to 1$ for large q, we scale $S(q)$ down to match the large q value of $\langle|\hat{\xi}_{\mathbf{q}}|^2\rangle$. For both the water and hydrocarbon surfaces, $S(q)$ obtained from the surface positions describes quite well the position as well as the relative height of the peaks in $\langle|\hat{\xi}_{\mathbf{q}}|^2\rangle$ except at the smallest q. The large q part of the spectrum therefore appears to be dominated by the in-plane structure

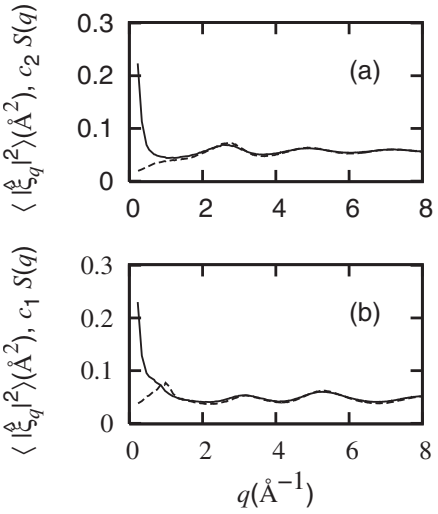

FIG. 5. Capillary-wave spectrum (solid line) and the in-plane structure factor $S(q)$ (dashed line) for the (a) water and (b) TMP surfaces as a function of wave vector q. The value of the constants are $c_1 = 1/21.5$ Å^2 and $c_2 = 1/17.6$ Å^2.

factor as expected. At small q the CW contribution to the spectrum dominates and deviation of $S(q)$ from the spectrum become noticeable. This is perhaps indicative of coupling between the capillary-wave and in-plane fluctuations. In light of the structure in $S(q)$ up to $q < 1.0$ Å^{-1}, a choice of L_m should be such that it excludes most of the local structure contribution to the calculated CW spectrum. The value of L_m estimated in Sec. IV A satisfies this requirement.

Turning to the spectrum for water in Fig. 4, there is a peak at $q \sim 3.2$ Å^{-1} in $\langle |\hat{\xi}_{\mathbf{q}}|^2 \rangle$ which corresponds to the pair separation between two oxygen atoms on hydrogen bonded molecular pairs. The peak height and position are quite insensitive to the hydrocarbon component, which changed from P to TMP in series 1. This insensitivity of the water surface was also observed in its intrinsic density profiles, orientation, and hydrogen bonding with respect to the hydrocarbon surface [12].

The spectrum for surface hydrocarbon sites is more interesting. For the *n*-pentane–water system, there is a peak at $q \sim 1.1$ Å^{-1}, which becomes less prominent in series 1 on going from *n*-pentane to 2,2,4-trimethyl pentane. This wave vector corresponds to structure on the surface at a length scale of ~5.5 Å, which is of the order of length of the hydrocarbon molecules in series 1. Terminal sites on molecules must be contributing to the set of surface sites. The presence of a peak would then suggest a preferential layering of these molecules at the surface, a trend observed for linear hydrocarbon-water interfaces [42]. An increase in hydrocarbon branching reduces the peak height suggesting a reduction in layering due to branching. This is in agreement with observations based on orientational order of molecules and intrinsic density profiles. There are additional peaks at $q \sim 3.0$ and ~5 Å^{-1} corresponding to the distance between three and two connected carbon sites on a molecule. These peaks could arise due to part of the molecule contributing to the surface.

Series 2 shows a somewhat different trend than series 1. The peak at $q \sim 1.1$ Å^{-1} for P shifts to larger q for O. The larger size of *n*-octane makes it harder to stack up and form layers at the surface. Consequently, the number of sites that can contribute to the surface decreases and the peak shifts to large q, with respect to P. An increase in branching from O to TMP leads to a shift in the peak position to smaller q as well as broadens the peak which is the effect of decreasing the molecular size. This trend is analogous to that seen in intrinsic profiles and orientation of molecules at the surface for series 2.

With the CW spectrum available, model parameters can be extracted from a fit of the small q component of the spectrum to Eqs. (24) and (25), or Eqs. (29) and (30) for models 2 and 3, respectively. Since model 3 requires a fit of the large q CW spectrum, which is dominated by the in-plane structure, a fit is likely to be misleading unless the in-plane fluctuations have been removed. Since we do not have a formal prescription for removing the noncapillary structure from this spectrum, we fit the water capillary spectrum to model 2. Recognizing that for an equilibrium interface, $\gamma_{A0} = \gamma_{B0}$ and $K_1 = K_2$, we fit the CW spectrum to Eq. (24) and obtain parameters which are presented in Table I.

The values of surface tension extracted from the fit (γ_{fit}) for all interfaces are in good agreement with the corresponding values obtained from the molecular virial (γ_{sim}), although they are slightly overestimated. While the estimates for K_{AB} show an apparent increase with increase in branching at a fixed chain length for series 1 hydrocarbons as well as an increase with reduced branching for constant molecular mass, we refrain from assigning a physical interpretation for this trend. The magnitude of K_{AA} does not show any systematic trends.

From the model parameters obtained from the fits, Eq. (26) allows for the calculation of the predicted value of the CW broadened surface width, σ_p^2. This width is presented in Table I and is in good agreement with the widths obtained from the distribution of surface positions. The good agreement between surface tension and widths as obtained through the fits with simulation data for all five water-hydrocarbon interface validates the applicability of model 2 to such liquid-liquid interfacial systems.

In order to make a comparison of the surface tension predicted by the model with the independent estimate from the simulation, we estimate the capillary-wave contribution to the surface tension based on Eq. (40). An input quantity for the calculation of γ_{CW} is the bulk correlation length of the hydrocarbon and water phases. Additional simulations were performed for the bulk liquid phase based on which the site-site pair correlation functions were calculated. Since the $l_{0,A}$ and $l_{0,B}$ values enter Eq. (40) through the logarithm, the absolute magnitudes are not very important [47] and an approximate value is estimated by calculating the average of all site-site pair correlation lengths. For water we use a correlation length of 4.0 Å while the values for different hydrocarbons are listed in Table I. The capillary-wave correction to the bare surface tension is negative for all interfaces simulated and the predicted surface tension γ_p values for all systems are obtained and listed in Table I. The predicted surface tension values are found to be in good agreement with the independent simulation estimates, γ_{sim}.

A key prediction of model 2 is a finite interfacial width in the thermodynamic limit ($L \to \infty$). Size dependence studies

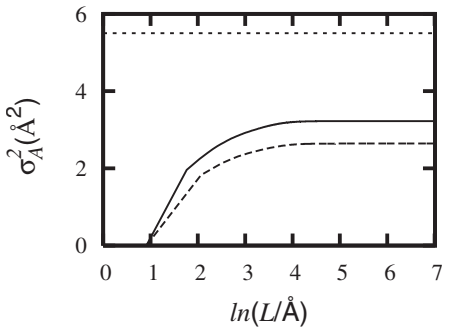

FIG. 6. Variation of the CW contribution to width with L for the water surface at the water–n-octane interface. (a) Prediction of model 2 (solid line). (b) Prediction of model 2 using the experimental surface tension value (large dashes). (c) Experimental estimate for an interface with size 100×80 mm (small dashes).

based on molecular simulations [6] support a width proportional to the logarithm of L that increases with L for sizes accessible in simulations. Therefore, it would be useful to study the L dependence of σ_A^2 or σ_B^2 and check for qualitative consistency with previous studies. Furthermore, an estimate of the width predicted by our model in the large L limit can be compared with experimental measurements for the same systems, when available, thereby allowing for experimental verification.

Model parameters obtained from the simulation are used to calculate the L-dependent width for the water surface of the water$-n$-octane interface beyond what is accessible in our simulation and the estimates are presented in Fig. 6. For small L, the width increases linearly with the logarithm of L consistent with previous studies [6]. For length scales of the order of a millimeter, the CW contribution to the width has already reached a constant value of ~3.32 Å. Since there is no published experimental data on size dependence of width for this system, we take the data of Mitronovic *et al.* [41] for a water–n-octane system with an area of cross section of 100 mm $\times$ 80 mm as a reference. The predicted width is found to be roughly 1.71 times smaller than the experimental estimate of 5.5 Å [41] for the total interfacial width. Clearly for this system not only does the width stay finite in the large L limit, it has the same order of magnitude as experimental estimates. It should be noted that the experimental estimate for interfacial width includes the CW as well as the intrinsic width and the CW contribution alone is of the order of 3.5 Å [41], which is in better agreement with the values estimated here.

The difference in the calculated and experimental widths could be due to different procedures employed for width estimation besides being a reflection of the shortcomings of the force field and perhaps also the approximate treatment of electroststic interactions used [37], in our simulations. The surface tension value for this system in our simulation, ~36 mN/m, is much smaller than the experimental value of ~52 mN/m, suggesting a need for a better force field and more accurate treatment of electrostatic interactions. Keeping all model parameters fixed at the values obtained from the simulation and changing the magnitude of surface tension to its experimental value, the predicted L dependence is presented in Fig. 6. A change of surface tension value does not affect the qualitative behavior of σ_A^2 but it brings its large L magnitude down to ~2.65 Å, which makes the agreement with the reference experimental value slightly worse. It is conceivable that with a better force field and improved simulation methodology, better estimates of the widths in the large L limit can be obtained based on the model.

V. SUMMARY

The CWM for liquid-vapor interfaces is modified for liquid-liquid interfaces by treating them as two interacting surfaces. The introduction of a two-surface representation of the interface is motivated by the observation that the Gibbs surfaces for the two immiscible liquids forming the interface usually do not overlap and a physically relevant Gibbs surface for the system cannot be identified. Model 1 approximates the interactions between the two surfaces as harmonic. The resulting expressions for the CW broadened widths diverge in the thermodynamic limit and require a small length scale cutoff, L_m, above which the model can be applied analogous to the liquid-vapor CWM.

The presence of a bulk phase next to the liquid surface is expected to damp surface fluctuations. These surface-bulk interactions are incorporated in model 2, which treats them as harmonic to lowest order. The resulting CW broadened widths for the two surfaces do not diverge in the thermodynamic limit unlike model 1 and the liquid-vapor CWM. The introduction of a small length scale cutoff is still necessary.

For the liquid-vapor CWM, inclusion of curvature corrections to the Hamiltonian leads to a width that vanishes in the limit of vanishing surface area [26]. We therefore include curvature corrections in model 3 for the liquid-liquid interface. The resultant CW broadened width does not diverge in the thermodynamic limit and also remains finite for a vanishing surface area.

The number of additional parameters beyond the liquid-vapor CWM was kept to a minimum by formulating a purely harmonic model. This is, of course, an approximation and there exists a scope for improving the models. The degrees of freedom associated with structure of the surface layer are excluded. It might be possible to extend this work by making a connection with liquid-state theories and a density-functional formulation will be presented in a subsequent publication.

In order to test the predictions of the models proposed here, MD simulations are performed for a series of water-hydrocarbon interfaces. A procedure to identify the surface atomic sites is utilized and the set of surface sites so obtained is analyzed. Models 1 and 2 require a small length scale cutoff, L_m, above which the model can be applied. In the absence of a theoretical criterion for estimating its value, we estimate L_m as the length scale below which bulk contributions to surface fluctuations dominate the CW contribution. The interface is coarse grained in order to study the length scale dependence of bulk and CW contributions to the width. Estimated values of L_m are found to be of the order of twice the equilibrium carbon-oxygen nearest-neighbor separation. A lateral size (L) dependence study of the two contributions

to surface fluctuations from independent simulations, such as the one performed by Senapati *et al.* [6], would be particularly useful.

With L_m available, the CW spectrum is obtained numerically. This spectrum shows the usual rapid decrease at small wave vectors expected from CW models but the large q part is found to resemble the in-plane structure factor obtained from the surface sites. The spectrum fits the predictions of model 2 well and model parameters are extracted. Fitted values of surface tension are found to be in good agreement with estimates based on the virial. The CW broadened width predicted by model 2, based on the fitted model parameters, is also found to compare favorably with values obtained independently from the distribution of surface sites. Furthermore, the CW correction to the bare surface tension is negative and brings down the value of the bare surface tension closer to the independent estimate of the systems surface tension. In light of the small magnitude of the CW correction to the surface tension, the bare surface tension can be taken as an upper bound to the macroscopic surface tension and a comparison of the bare surface tension with the macroscopic surface tension should be reasonable. These observations about the surface width and surface tension predicted by model 2 confirm its applicability to such liquid-liquid interfaces.

The dependence of water-hydrocarbon interfacial properties on the extent of hydrocarbon branching is studied in terms of the model parameters and CW spectrum. For the same molecular architecture, the interface formed by the longer hydrocarbon molecule has a higher surface tension. This is manifested in smaller CW broadened widths and larger separation between the centers of the surface layers, L_0. The CW spectrum for the hydrocarbon interface reveals a peak at small q corresponding to molecular lengths indicating layering for the smaller hydrocarbons. This layering has also been noticed in our preceding study of the intrinsic structure and orientation of these water-hydrocarbon interfaces [12]. The CW spectrum, or equivalently, the wave-vector-dependent height-height correlation function, appears to be a direct probe of interfacial structure. In light of recent experimental observation of CW fluctuations on colloidal surfaces [48], this might be a fruitful direction for probing interfacial structure.

For liquid-vapor interfaces, where a single-surface approximation is used, a wave-vector-dependent surface tension can be obtained from the capillary-wave spectrum and is measurable in diffuse x-ray scattering experiments. It would be useful to obtain expressions for the differential cross section for diffuse x-ray scattering from liquid-liquid interfaces in terms of the CW models presented here, possibly interpret experimental data based on them, and extract model parameters from experiments. Finally, in future work we will attempt to incorporate the ideas presented in the context of liquid-liquid interfaces to liquid-vapor and liquid-solid wall interfaces.

ACKNOWLEDGMENTS

This work was supported by the DOE Grant No. DE-FG03-0ZER15376 and by the NSF Grant No. CHE 0608640.

[1] J. S. Rowlinson and B. Widom, *Molecular Theory of Capillarity* (Clarendon Press, Oxford, 1982).
[2] F. Buff, R. Lovett, and F. Stillinger, Phys. Rev. Lett. **15**, 621 (1965).
[3] M. Requardt and H. J. Wagner, J. Stat. Phys. **64**, 807 (1991).
[4] J. D. Weeks, J. Stat. Phys. **64**, 823 (1991).
[5] I. Benjamin, Annu. Rev. Phys. Chem. **48**, 407 (1997).
[6] S. Senapati and M. L. Berkowitz, Phys. Rev. Lett. **87**, 176101 (2001).
[7] J. D. Weeks, J. Chem. Phys. **67**, 3105 (1977).
[8] J. P. Nicolas and N. R. de Souza, J. Chem. Phys. **120**, 2464 (2004).
[9] H. A. Patel, E. B. Nauman, and S. Garde, J. Chem. Phys. **119**, 9199 (2003).
[10] E. Chacon and P. Tarazona, Phys. Rev. Lett. **91**, 166103 (2003).
[11] P. Tarazona and E. Chacon, Phys. Rev. B **70**, 235407 (2004).
[12] J. Chowdhary and B. M. Ladanyi, J. Phys. Chem. B **110**, 15442 (2006).
[13] D. Michael and I. Benjamin, J. Phys. Chem. **99**, 1530 (1995).
[14] M. Natalia and D. S. Cordeiro, Mol. Simul. **29**, 817 (2003).
[15] Y. Zhang, S. E. Feller, B. R. Brooks, and R. W. Pastor, J. Chem. Phys. **103**, 10252 (1995).
[16] R. F. Kayser, Phys. Rev. A **33**, 1948 (1986).
[17] J. D. Weeks and W. van Saarloos, J. Phys. Chem. **93**, 6969 (1989).
[18] S. K. Sinha, E. B. Sirota, S. Garoff, and H. B. Stanley, Phys. Rev. B **38**, 2297 (1988).
[19] D. G. Triezenberg and R. Zwanzig, Phys. Rev. Lett. **28**, 1183 (1972).
[20] W. Helfrich, Z. Naturforsch. C **24**, 693 (1973).
[21] K. R. Mecke and S. Dietrich, Phys. Rev. E **59**, 6766 (1999).
[22] C. Fradin, A. Braslau, D. Luzat, D. Smilgies, M. Alba, N. Boudet, K. Mecke, and J. Daillant, Nature (London) **403**, 871 (2000).
[23] D. Li, B. Yang, B. Lin, M. Meron, J. Gebhardt, T. Graber, and S. A. Rice, Phys. Rev. Lett. **92**, 136102 (2004).
[24] S. Mora, J. Daillant, K. Mecke, D. Luzet, A. Braslau, M. Alba, and B. Struth, Phys. Rev. Lett. **90**, 216101 (2003).
[25] J. Stecki, J. Chem. Phys. **109**, 5002 (1998).
[26] A. Milchev and K. Binder, Europhys. Lett. **59**, 81 (2002).
[27] R. L. C. Vink, J. Horbach, and K. Binder, J. Chem. Phys. **122**, 134905 (2005).
[28] M. Müller and L. G. MacDowell, Macromolecules **33**, 3902 (2000).
[29] I. Benjamin, J. Chem. Phys. **97**, 1432 (1992).
[30] J. K. Percus, in *Fluid Interfacial Phenomena*, edited by C. A. Croxton (John Wiley, New York, 1986), pp. 1–44.
[31] J. V. Sengers and J. M. J. van Leeuwen, Phys. Rev. A **39**, 6346 (1989).

[32] H. J. C. Berendsen, J. R. Grigera, and T. P. Straatsma, J. Phys. Chem. **91**, 6269 (1987).
[33] W. Allen and R. L. Rowley, J. Chem. Phys. **106**, 10273 (1997).
[34] W. L. Jorgensen, J. D. Madura, and C. J. Swenson, J. Am. Chem. Soc. **106**, 6638 (1984).
[35] M. P. Allen and D. J. Tildesley, *Computer Simulation of Liquids* (Oxford University Press, Oxford, 1989).
[36] P. Demontis, S. Spanu, and G. B. Suffritti, J. Chem. Phys. **114**, 7980 (2001).
[37] D. Wolf, P. Keblinski, S. R. Phillpot, and J. Eggebrecht, J. Chem. Phys. **110**, 8254 (1999).
[38] D. Zahn, B. Schilling, and S. M. Kast, J. Phys. Chem. B **106**, 10725 (2002).
[39] H. J. C. Berendsen, J. P. M. Postma, W. F. van Gunsteren, A. DiNola, and J. R. Haak, J. Chem. Phys. **81**, 3684 (1984).
[40] H. Matsubara, M. Murase, Y. H. Mori, and A. Nagashima, Int. J. Thermophys. **9**, 409 (1988).
[41] D. M. Mitrinovic, A. M. Tikhonov, M. Li, Z. Huang, and M. L. Schlossman, Phys. Rev. Lett. **85**, 582 (2000).
[42] J. L. Rivera, C. McCabe, and P. T. Cummings, Phys. Rev. E **67**, 011603 (2003).
[43] M. Müller and G. Münster, J. Stat. Phys. **118**, 669 (2005).
[44] A. Werner, F. Schmid, M. Müller, and K. Binder, Phys. Rev. E **59**, 728 (1999).
[45] J. Chowdhary and B. M. Ladanyi, J. Phys. Chem. B (to be published)
[46] J. Stecki, J. Chem. Phys. **120**, 3508 (2004).
[47] D. Michael, and I. Benjamin, J. Electroanal. Chem. **450**, 335 (1998).
[48] D. G. A. L. Aarts, M. Schmidt, and H. N. W. Lekkerkerker, Science **304**, 847 (2004).